博士学位論文

Influence of the Gulf Stream on ascending airstreams in extratropical cyclones

(メキシコ湾流による温帯低気圧の上昇気流への影響)

氏名

Jinyoung Son

北海道大学大学院理学院

自然史科学専攻

2023 年 3 月

Abstract

The Gulf Stream plays an important role in the development of atmospheric phenomena over the North Atlantic. This study investigates the effects of the Gulf Stream on the air-parcel trajectories of ascending air streams in extratropical cyclones (ETCs). These trajectories are referred to as ETC's ascending air-parcel trajectories (EAA trajectories). The EAA trajectories are analyzed by using two numerical experiments of an atmospheric general circulation model (AGCM) for 20-year winter from December 1981 to February 2001: one with daily observational sea surface temperature (SST) data called CNTL and the other with smoothed SST data over the Gulf Stream SST front called SMTHG. The EAA trajectories are identified as trajectories that ascend across the 900 hPa surface, which roughly corresponds to the top of the marine atmospheric boundary layer, near ETCs. It is found that EAA trajectories occur more frequently at 900 hPa level along the Gulf Stream current axis after its separation from the coast in CNTL than in SMTHG. The EAA trajectories crossing the 900 hPa height in this region are referred to as frontal EAA trajectories. Frontal EAA trajectories in the CNTL experiment reach higher altitudes than those in SMTHG, and travel longer horizontal distances. About two-thirds of the larger ascent of frontal EAA trajectories in CNTL than in SMTHG is explained by the effect of the diabatic heating. During the ascent phase, the diabatic heating of EAA trajectories in CNTL is stronger than that of SMTHG. Before ascending in the free troposphere, the frontal EAA trajectories are more strongly warmed through the sensible heat flux and moistened via the latent heat flux by the Gulf Stream in CNTL than in SMTHG. The additionally supplied moisture in CNTL than in SMTHG is used as the latent heat release, resulting in stronger ascending motion of frontal EAA trajectories. These results highlight that the Gulf Stream plays an important role in ascending air streams in ETCs over the North Atlantic.

Table of Contents

1. Introduction

Western boundary currents that have a strong sea surface temperature (SST) front are important for air-sea interaction in midlatitude (Small et al. 2008; Kwon et al. 2010; Minobe et al. 2010). These currents transport warm water from the lower latitudes and release a large amount of heat and moisture to the atmosphere over the midlatitude ocean (Kuwano-Yoshida et al. 2010; Ogawa and Spengler 2019; Tsopouridis et al. 2020). The western boundary currents strengthen near-surface wind convergence, precipitation, and upward winds along the SST fronts (Minobe et al. 2008; Shimada and Minobe 2011; Small et al. 2019; Masunaga et al. 2020). Also, these ocean currents influence several atmospheric phenomena such as extratropical cyclones (ETCs; Nakamura et al. 2012; Kuwano-Yoshida and Minobe 2017; Zhang et al. 2019), storm tracks (Wilson et al. 2009; Brayshaw et al. 2011; Ogawa et al. 2012; Small et al. 2014; Piazza et al. 2016; Ma et al. 2017) and atmospheric blocking (O'Reilly and Czaja 2015; O’Reilly et al. 2016; Joyce et al. 2019; Yamamoto et al. 2021). Especially, ETCs are important because they affect the formation of storm tracks and atmospheric blocking (Steinfeld and Pfahl 2019; Priestley and Catto 2022).

In ETCs, there are ascending airstreams that are related to precipitation and intensification of cyclones, strong and well-organized ascending airstreams in ETCs are called the warm conveyor belt (WCB; Booth et al. 2012; Binder et al. 2016). The WCB is a warm and moist airstream that rises coherently from the marine atmospheric boundary layer (MABL) to the upper troposphere in ETCs (Browning 1986). During the development of WCB, WCB transports materials from the MABL to the upper troposphere and is also important for the horizontal movement of materials as well as vertical direction (Wernli and Davies 1997; Stohl 2001; Sinclair et al. 2008; Joos and Forbes 2016; Oertel et al. 2019). In the Northern Hemisphere, WCBs mainly originate in the western North Atlantic and the western North Pacific, where the western boundary currents, i.e., the Gulf Stream and the Kuroshio, respectively flow (Eckhardt et al. 2004; Madonna et al. 2014). In particular, moisture that causes latent heating, which is important for the development of WCBs, is supplied to WCBs and mainly occurs around the western boundary currents in the Northern hemisphere (Boutle et al. 2010; Pfahl et al. 2014; Schäfler and Harnisch 2015).

The previous studies showed that the Lagrangian method is quite useful for detecting, analyzing, and understanding airstreams (Wernli and Davies 1997; Madonna et al. 2014; Hirata et al. 2015; Sheldon et al. 2017; Yamamoto et al. 2021), but only a few previous studies investigated the influence of western boundary currents using the Lagrangian method. Sheldon et al. (2017) conducted five-day regional atmospheric model experiments with observed and smoothed SSTs and found that the Gulf Stream SST front enhanced the ascent of WCBs. Hirata et al. (2015) used a regional atmosphere-ocean coupled model for three-day integration and reported that the Kuroshio strongly contributed to supplying moisture to the WCBs based on a three-day numerical experiment. Recently, Yamamoto et al. (2021) tracked air parcel trajectories for 31 years of wintertime by using a reanalysis dataset for the role of latent heating in atmospheric blocking. Although these studies demonstrated that the Lagrangian method is quite effective in understanding the roles of the western boundary currents on air streams, the small number of studies leaves room for further development. In particular, it should be useful to evaluate the roles of western boundary currents on air streams in ETCs by using 10-year or longer numerical experiments to know the long-term averaged influence on a Lagrangian framework rather than Eulerian framework employed by previous studies of long-term numerical experiments (Small et al. 2014; Piazza et al. 2016)

Therefore, this study aims to quantify the effects of the western boundary currents on ascending airstreams, including WCBs, in ETCs over a long time and to clarify the mechanism of how the western boundary currents affect airstreams in ETCs. To this end, this study analyzes 20-year atmospheric general circulation model (AGCM) experiments because more than hundreds of ETCs, a phenomenon of synoptic scale, can be analyzed.

The rest of the present paper is organized as follows. In section 2, the model configuration, experiment design, and analysis method are described. Section 3 presents the spatio-temporal structure and development mechanism of ETC's ascending air-parcel trajectories (EAA trajectories) in two AGCM experiments. A discussion and conclusions are presented in section 4.

2. Data and Method

2a Data

In this study, outputs of the AGCM for the Earth Simulator (AFES) version 3 (Ohfuchi et al. 2004; Enomoto et al. 2008; Kuwano-Yoshida et al. 2010) developed by the Japan Agency for Marine-Earth Science and Technology (JAMSTEC) presented by O'Reilly et al. (2016) are analyzed. This model has an approximately 50 km (T239) horizontal resolution and 48 vertical sigma levels. AFES employs the Emanuel convection scheme (Emanuel and Zivkovic-Rothman 1999). The initial conditions for AFES are taken from the Japanese 25-year Reanalysis Project (JRA-25; Onogi et al. 2007).

To investigate the effect of western boundary currents, the two experiments of the AFES are used. The first experiment referred to as the control experiment (CNTL), uses the 0.25° daily SST data provided by the National Oceanic and Atmospheric Administration (NOAA; Reynolds et al. 2007) for the bottom boundary condition. The second experiment uses the smoothed SST data around the Gulf Stream (85°–30°W, 25°–50°N) and is referred to as SMTHG. This SST data is smoothed by a 1-2-1 running mean filter in both the zonal and meridional directions 200 times. The two experiments of AFES are integrated for 20 years from 1 December 1981 to 3 March 2001. Figure 1 represents the averaged SST for 20-yr December-February (DJF) for CNTL, SMTHG, and CNTL−SMTHG. The difference in the SST between the two experiments is clear on the offshore of the central United States East coast (Fig. 1c). Previous papers studied the midlatitude air-sea interaction with observed and smoothed SSTs for multiple-year winter integration periods using AFES (O'Reilly et al. 2017; Kuwano-Yoshida and Minobe 2017; Tsopouridis et al. 2020) or other models (Small et al. 2014; Omrani et al. 2019; Vries et al. 2019), but none of them performed air-parcel tracking.

The variables of AFES are classified into two groups: 1. the variables averaged during 10 minutes before and after the output, 2. the variables averaged during 6 hours before and after the output time. The variables of the first group and second group output every 6 hours from 05:55 and 03:00 UTC 01 September 1981. The 3-dimensional winds, temperature, specific humidity, sea level pressure (SLP), and SST are the first groups. The variables of the second group are latent heating, radiative heating, vertical diffusion, and sensible and latent heat flux.

In addition to AFES outputs, the data of Fifth Generation ECMWF Reanalysis (ERA5; Hersbach et al. 2020) is employed in this study. The results of AFES are compared with those of ERA5. The resolution of ERA5 is approximately 31 km (TL 639) and there are 137 layers from the surface to 1 hPa. In this study, the data from 1 December 1981 to 3 March 2001 is used.

2b Air-Parcel Tracking

To obtain EAA trajectories, a large number of air parcel trajectories are tracked by using the Lagrangian Analysis Tool - version 2 (LAGRANTO; Sprenger and Wernli 2015). Tracking is a time-consuming calculation, and the amount of the calculation is determined by the number of air-parcel tracks and tracking time length. The number of tracks is given by the spatial coverage, spatial density, and temporal frequency of air-parcel starting points. The starting points are set at every 80 km and every 20 hPa within the layer from 1050 to 910 hPa and at every 6 hours from 05:55 UTC 01 December in a year to 23:55 UTC 28 or 29 February in the next year for 20 winters, and the tracking time length is 72 hours. These arrangements are essentially the same as those used by Madonna et al. (2014), but this study is interested in the interaction between air-parcels and ocean currents, so the height at which the starting points are arranged is lower than the previous study. Also, this study is interested in winter air-sea interaction, the starting time of air parcels is limited in the winter season. To know the appropriate spatial coverage of starting points for the present study, the entire Northern Hemisphere is used as an area of starting points for one winter firstly (December 1981-February 1982) using ERA5 data. Examining the one-winter air-parcel tracks, this study determined that an area from 100°W to 30°W and 15°N to 50°N for starting points is reasonable to retain the air-parcel tracks that come to the vicinity of the Gulf Stream. Based on the analyses for one winter, in AFES and ERA5, the air-parcels are tracked for 20 winter seasons. LAGRANTO provides air parcel position and the potential temperature (θ), specific humidity (q), and heating components as those positions.

To identify the EAA trajectories two procedures are applied for the largest ascent of 48 hours within 72-hour tracking. First, since this study is interested in ascending air-parcels associated with air-sea interaction, the trajectories that cross the 900 hPa surface upward during the 48 hours of the largest ascent are selected. The second procedure is to hold only trajectories that enter the area of ETCs at least once for the 48 hours of ascent. The area of ETCs is identified by a circular area with a radius of the length of 5°longitudes from the center of the cyclone, which is defined by local SLP minima. A radial cap of 5° radius is a criterion used by several studies about cyclones (Larson et al. 2005; Kunkel et al. 2010; Hawcroft et al. 2012; Scoccimarro et al. 2014; Vannière et al. 2020). Figure 2 shows the process for identifying the cyclone area. The local SLP minima are deemed to exist at any point at which the SLP is lower than all eight neighboring grid points (Wernli and Schwierz 2006, Fig. 2a). If several cyclone areas overlap, only the cyclone area that has the lowest SLP minimum is kept (Fig. 2b). The local SLP minimum must be smaller than 1000 hPa are determined as cyclone area (Fig. 2c). The local SLP minima identified on the south of 25°N are removed to exclude tropical cyclones. The cyclone areas remaining by these procedures are used to identify EAA trajectories.

Figure 3 shows an example of all trajectories and EAA trajectories starting at 17:55 UTC 08 December 1982. In this case, almost all EAA trajectories started over the ocean (Fig. 3d). After 24 hours from the tracking start, the positions of all trajectories are not related to the cyclone yet, but the EAA trajectories are located around the cyclone center (Figs. 3b and 3e). In Fig. 3c, the air parcels left the MABL to form a comma shape, while air parcels located in the MABL represent the pattern of an ascending phase of WCBs (Browning 1986; Schultz and Vaughan 2011). The EAA trajectories also form a comma shape, but there is no shape of an ascending phase of WCBs because the trajectories have already left the MABL (Fig. 3f). Also, EAA trajectories have split into an anticyclonically turning branch that goes east and a cyclonically turning branch that goes to the cyclone center. The pattern of the two branches is very similar to the movement of WCBs suggested by previous studies (Schultz and Vaughan 2011; Martínez-Alvarado et al. 2014). In particular, Schultz and Vaughan (2011) shows that the two branches of WCBs stand out after occlusion.

To know whether AFES reproduces EAA trajectories reasonably, the EAA trajectories of AFES are compared with those of ERA5. The EAA trajectories at 900 hPa are concentrated around the Gulf Stream SST front (Figs. 4a and 4b). Although the number of EAA trajectories in CNTL is 5.1 % larger than that of ERA5 because of the 4.3 % higher cyclone density in CNTL than in ERA5, the characteristic of the spatial distribution that the EAA trajectories leave the MABL along the Gulf Stream current axis is similar. Therefore, this study considers that the AFES reasonably represent EAA trajectories including the effect of the Gulf Stream on them.

Because this study is interested in the effect of the Gulf Stream on the EAA trajectories, trajectories that could be influenced by the Gulf Stream region are selected additionally. In this study, the Gulf Stream region is defined as an area where the upward wind at 850 hPa of CNTL is stronger than SMTHG by the effect of the Gulf Stream (Green box in Fig. 5). The EAA trajectories located in the Gulf Stream region at 900 hPa are selected as the EAA trajectories influenced by the Gulf Stream region. These trajectories are called frontal EAA (FEAA) trajectories.

2C. Diagnostics of Ascending Motion

An ascent of FEAA trajectories is diagnosed by dividing it into an adiabatic ascent and a diabatic ascent during 48 hours of the largest ascent starting below 900 hPa. During the 48 hours ascent of a trajectory, the difference between the minimum and maximum altitudes is the total ascent. The adiabatic ascent is given by the difference in altitude at the horizontal location of the maximum altitude between the maximum altitude and the altitude of the same potential temperature surface as that at the lowest altitude position. The diabatic ascent is defined as the difference between the total ascent and the adiabatic ascent.

The diabatic ascent is related to the diabatic heating in FEAA trajectories. In this study, the definition of diabatic heating is the sum of cumulus heating, large-scale heating, longwave heating, shortwave heating, and vertical diffusion. These components for each trajectory are also obtained by using LAGRANTO. Diabatic heating should be able to explain the change of simulated potential temperature, θ, in FEAA trajectories. Figure 6 represents the time evolution of θ on the average of all 20-yr FEAA trajectories with 0 hours as the start time of trajectories. The θ by diabatic heating is calculated by the following equation:

$$\widehat{\theta_Q}(t) = \theta(t_0) + \int_{t_0}^{t} \frac{Q(\tau)}{c_p} d\tau, \quad (1)$$

where $\theta(t_0)$ is the potential temperature at the starting point and $\widehat{\theta_Q}$ is the estimated potential temperature due to diabatic heating added to $\theta(t_0)$. Q is the diabatic heating and C_p is the specific heat capacity of air at constant pressure. The simulated and estimated potential temperatures are not completely the same, but the difference is within 0.2 % at all times. Therefore, there is no significant problem with the analysis of diabatic heating in this study.

3. Results

3a Spatio-temporal structures

Figures 4b – 4d show the spatial distribution of EAA trajectories at 900 hPa for 20 winter seasons in CNTL, SMTHG, and the difference between the two experiments. The density of EAA trajectories is high above the Gulf Stream current axis, which corresponds to the southern end of the Gulf Stream SST front (Fig. 4e). Over this high-density region, time-averaged upward winds occur, accompanied by the Gulf Stream rainband (Minobe et al. 2010). The difference in the density of EAA trajectories between CNTL and SMTHG is also concentrated over the Gulf Stream current axis (Fig. 4d). Although the number of FEAA trajectories of CNTL is only 4.0 % larger than in SMTHG, this difference is still statistically significant ($p < 0.03$) according to the Wilcoxon rank-sum test using the weekly counted number of FEAA trajectories.

The different distribution of FEAA trajectories between CNTL and SMTHG can be related to the different cyclone distributions between the two experiments. Figure 7 shows the difference in the cyclone frequency calculated by dividing the difference in the number of cyclones between CNTL and SMTHG by the number of cyclones in SMTHG. The cyclone frequency of CNTL is higher on the Gulf Stream than SMTHG, especially around 60°W and 40°N by more than 20 %. The difference in the cyclone frequency between the two experiments further south than 35°N is not reliable because the number of cyclones is too small in both CNTL and SMTHG. Kuwano-Yoshida et al. (2010) suggested that there is no conclusive evidence that the Gulf Stream affects the eddy activity over the North Atlantic through 5 years AGCM experiments. However, there is a statistical difference in the cyclone frequency between CNTL and SMTHG for 20 winter seasons over the North Atlantic in this study (Yellow contours of Fig. 7). This result agrees with a previous study suggesting that 20 years is sufficient to identify significant responses in the North Atlantic region (Rodwell et al. 2004). The difference in the cyclone frequency between the two experiments is similar to the difference in the density distribution of EAA trajectories between the two experiments in Fig. 4d. These results suggest that the difference in the cyclone frequency by the Gulf Stream may have affected the density distribution of EAA trajectories.

The vertical and horizontal movement of EAA trajectories is examined because the occurrence of FEAA trajectories is related to the movement of air parcels. The reached height of FEAA trajectories is defined as the highest height within 48 hours after trajectories cross 900 hPa for the first time. The trajectories having less than 48 hours recorded after the 900 hPa crossing, i.e., the crossing occurs more than 24 hours after the tracking began with the 72-hour tracking period, were excluded from this analysis.

Figure 8 represents the number of trajectories as a function of the reached height for FEAA trajectories and non-frontal EAA trajectories, which are EAA trajectories that are not located in the Gulf Stream region at 900 hPa. The number of FEAA trajectories increases with the reached height of trajectories until 300 hPa in both CNTL and SMTHG (Fig. 8a). The difference in the number of FEAA trajectories is the largest from 250−300 hPa and the number of FEAA trajectories reached above 300 hPa is 31 % larger in CNTL than in SMTHG. The FEAA trajectories that reach the upper troposphere (400 hPa) are also larger 15 % in CNTL than in SMTHG.

The reached height of non-frontal EAA trajectories shows a different distribution compared to FEAA trajectories (Fig. 8b). There is no difference in the number of non-frontal EAA trajectories above 300 hPa between CNTL and SMTHG, while there is an outstanding difference in FEAA trajectories. Also, the reached height of non-frontal EAA trajectories is relatively lower than that of FEAA trajectories in both CNTL and SMTHG. This result means that Gulf Stream intensifies the upward motion of ascending airstreams started under the MABL.

Previous studies showed that the strong ascending airstream in ETCs can reach even the stratosphere (Stohl 2001; Eckhardt et al. 2004; Madonna et al. 2014). To investigate the effect of the Gulf Stream on the ascent of FEAA trajectories to the stratosphere, the FEAA trajectories that reached the stratosphere are selected. The FEAA trajectories having 2 PVU (1 PVU = 10^{-6} Km^2 kg^{-1} s^{-1}) at above 600 hPa for 48 hours of ascent are identified as the FEAA trajectories that reached the stratosphere. The number of FEAA trajectories that reached the stratosphere is 22 % larger in CNTL than in SMTHG (Table 1). This result shows the Gulf Stream contributes to reaching the stratosphere of the airstream started under the MABL of the North Atlantic.

In addition to the vertical movement of FEAA trajectories, the horizontal movement is also investigated. The horizontal movement of EAA trajectories is investigated by using the maximum horizontal distance defined as the maximal distance from a point where the trajectory crosses 900 hPa for the first time within 48 hours from the crossing. Figure 9 represents the number of trajectories as a function of the maximum horizontal distance for FEAA trajectories and non-frontal EAA trajectories. A remarkable feature is that the number of FEAA trajectories that traveled more than 3000 km is 24 % larger in CNTL than in SMTHG (Fig. 9a). Furthermore, the FEAA trajectories of CNTL show a bimodal distribution, which is less prominent SMTHG. In non-frontal EAA trajectories, there is no significant difference in the distribution between the two experiments (Fig. 9b).

The FEAA trajectories of CNTL reach higher levels and move a greater distance than that of SMTHG. Because the horizontal wind becomes stronger at higher altitudes, the relation between reached height and the movement distance of FEAA trajectories is investigated. The movement distance and the reached height of the FEAA trajectories have a

Pearson correlation coefficient of about 0.5 in both CNTL and SMTHG. These results suggest that the presence of the Gulf Stream SST front intensifies the upward motion of FEAA trajectories and increases the movement distance of FEAA trajectories by raising the air parcels to a higher altitude where the wind is stronger.

3b Mechanisms of Ascending Motion

Previous studies demonstrated that diabatic heating is an important factor in the ascent of airstreams in ETCs (Madonna et al. 2014; Martínez-Alvarado et al. 2014; Joos and Forbes 2016). Table 2 represents the average adiabatic and diabatic ascent of FEAA trajectories in the two experiments of this study. The 68 % of the difference in the ascent of FEEA trajectories between CNTL and SMTHG, 12.3 hPa, is due to the diabatic heating. This result suggests that the diabatic process plays an important role in the difference in the ascent of the FEAA trajectories between CNTL and SMTHG. To understand the effect of the Gulf Stream on the diabatic heating of FEAA trajectories, each component consisting of diabatic heating is investigated.

Figure 10 shows an increasing rate in potential temperature (θ), the time evolution of each diabatic heating component, and an increasing rate in specific humidity (q) in the average of all FEAA trajectories. The temporal change of θ in FEAA trajectories of CNTL reaches its maximum at $t = 0$ h (Fig. 10a). In this change, latent heating plays a dominant role among three diabatic heating components, i.e., latent heating (sum of cumulus and large-scale heating), radiative heating (sum of longwave and shortwave heating), and heating by vertical diffusion. A decrease in q also demonstrates that the latent heating is active during the ascent phase of FEAA trajectories (Fig. 10b). This time evolution of diabatic heating for FEAA trajectories of CNTL is similar to that of SMTHG, but the diabatic heating is smaller in SMTHG than CNTL at all times from −24 hours to 14.5 hours (Fig. 10c). The diabatic heating of FEAA trajectories in CNTL is stronger 18 % than that of SMTHG from −24 to 14.5 hours. After t = 0 h, the latent heating dominates in the difference in the diabatic heating between CNTL and SMTHG, but the vertical diffusion is important in the difference in the diabatic heating before t = 0 h. Consistent with the strong latent heating after t = 0 h, a larger amount of water vapor is consumed in the FEAA trajectories of CNTL than in SMTHG (Fig. 10d). These results mean that the FEAA trajectories are heated by sensible heat before t = 0 h, and after t = 0 h, it is heated by the heat released by condensation of water vapor obtained from below the MABL.

The latent heating and vertical diffusion are important in the difference in the development of diabatic heating in FEAA trajectories. Therefore, we examined the time evolution of the sensible and latent heat flux that affects vertical diffusion and the supplying water vapor to FEAA trajectories. Figure 11 represents the time evolution of sensible and latent heat fluxes, at the horizontal position of trajectories, and the time derivative of q in FEAA trajectories. The sensible heat flux of FEAA trajectories is always stronger in CNTL than in SMTHG from −24 hours. The difference in the sensible heat flux of FEAA trajectories between the two experiments peaks at −6 hours and starts to decrease. This time evolution of difference in the sensible heat flux is similar to that of vertical diffusion shown in Fig 10c. This result suggests that the sensible heat flux is likely to influence directly the heating by vertical diffusion.

The latent heat flux of CNTL is also always higher than SMTHG from t = −24 hours to 0 hours. The difference in the latent heat flux is maximum at t = −4 hours and starts to decrease. As the latent heat flux of CNTL in FEAA trajectories becomes stronger than SMTHG, the difference in the dq/dt in FEAA trajectories between CNTL and SMTHG also increases. This means that the stronger evaporation in CNTL than in SMTHG is closely related to the larger supply of water vapor in FEAA trajectories of CNTL.

To investigate how evaporation and sensible heat flux affect the time derivative of specific humidity and vertical diffusion, the contribution of heat fluxes to each component is calculated. For this calculation, a space consisting of unit area (1 m^2) and height from the surface to the MABL (100 hPa) is assumed. The contribution of evaporation to the time derivative of specific humidity is calculated under the assumption that the evaporation affects the entire unit volume uniformly. The evaporation from the ocean is estimated from latent heat flux. The increase of specific humidity by evaporation between two experiments (Δq_{LHF}) is calculated by the following equation: $\Delta q_{LHF} = \frac{W_{LHF} \times \Delta t}{28.94 \times \rho}$

where W_{LHF} is the difference in the average latent heat flux at the horizontal position of FEAA trajectories for 23.5 hours between CNTL and SMTHG, ρ is the density of air. and Δt is period represented as second. The 28.94 is the conversion factor from mm/day to W/m^2 (Li et al. 1998). The stronger evaporation in CNTL than in SMTHG increases by 0.90 g/kg of q for 23.5 hours in unit volume, while the specific humidity of FEAA trajectories in CNTL only increased 0.23 g/kg than that of SMTHG for 23.5 hours. The increase in specific humidity due to stronger evaporation in CNTL than in SMTHG, which is about 4 times greater than the difference in specific humidity of FEAA trajectories between the two experiments, is sufficient to explain the difference in specific humidity of FEAA trajectories between the two experiments, even considering the loss of water vapor due to condensation. The latent heating by condensation results in an increase in temperatures and the increased temperature can intensify vertical diffusion. Therefore, if the reason for less increase of specific humidity in FEAA trajectories than an increase of specific humidity by evaporation is the condensation of water vapor, the latent heat also can intensify the vertical diffusion as a result.

If the sensible heat flux affects the unit volume uniformly and is transformed to the vertical diffusion, the vertical diffusion by sensible heat flux (D_{SHF}) is obtained by the following equation: $D_{SHF} = \frac{W_{SHF} \times \Delta t}{C_p \times \rho}$

Where W_{SHF} is the difference in the average sensible heat flux at the horizontal position of FEAA trajectories for -24 h to -0.5 h between CNTL and SMTHG, and Δt is period represented as second. C_p is the specific heat capacity of air at constant pressure and ρ is the density of air. For 23.5 hours, the integrated heating by stronger sensible heat flux in CNTL than in SMTHG is 0.78K, which is 54 % of the difference in the integrated heating of the FEAA trajectories by vertical diffusion between CNTL and SMTHG. The other 46 % is probably closely related to heating by condensation of water vapor in MABL.

The results shown above indicate that moisture uptake of air parcels in the MABL. The difference in q of FEAA trajectories between CNTL and SMTHG is almost 0 at $t = -24$ h and maximum at $t = -0.5$ h (Fig. 12). To investigate what happened during this time, the spatial distribution and average water vapor of FEAA trajectories at $t = -12$ h, the middle time when q increase, are investigated. At $t = -12$ h, FEAA trajectories of CNTL are already located around the Gulf Stream current axis (Fig. 13a). The number of FEAA trajectories of CNTL is mainly higher in the southwestern of 55°W and 43°N than in SMTHG, while that of SMTHG is higher southeastern of 55°W and 43°N than in CNTL (Fig. 13b). The distribution of the average humidity of the FEAA trajectories present at each grid point in CNTL is closely related to SSTs because they are located under the MABL at $t = -12$ h (Fig. 13c). Unlike the difference in the density distribution of FEAA trajectories, areas with larger water vapor of FEAA trajectories in CNTL than that of SMTHG are distributed east of 55°W (Fig. 13d).

To clarify which of the difference in the density distribution or distribution of average water vapor is more important to the difference in water vapor of FEAA trajectories between CNTL and SMTHG, the contribution of the 4 areas to the difference in the q of FEAA trajectories between CNTL and SMTHG at $t = -12$ h is calculated. To this calculation, the Gulf Stream region is divided into 4 areas centered on the 55°W and 43°N lines of Figs. 13b and 13d. The contribution in each quadrant is calculated by the following equation: $\frac{\sum_x \sum_y ratio(x,y) \times q(x,y)\ of\ CNTL - \sum_x \sum_y ratio(x,y) \times q(x,y)\ of\ SMTHG}{the\ difference\ in\ the\ averaged\ q\ between\ CNTL\ and\ SMTHG\ at\ t = -12\ h}$ where *ratio*(x,y) is the ratio of the number of FEAA trajectories at each grid point to all FEAA trajectories and $q(x,y)$ is the averaged q of FEAA trajectories at each grid point of t = −12 h. The contribution of quadrants 1 to 4 to the difference in the average q of all FEAA trajectories at t = −12 h between CNTL and SMTHG is about 0.8 %, 0.1 %, 116 %, and −16 %, respectively. The effect of quadrants 1 and 2 is very small because the density of FEAA trajectories is low in these two regions. The larger water vapor of FEAA trajectories in CNTL than that of SMTHG is entirely due to the 3rd quadrant where the density of FEAA trajectories in CNTL is higher than in SMTHG. In the 4th quadrant, the average water vapor of FEAA trajectories is higher in CNTL than in SMTHG, which is consistent with the difference of the average water vapor over 20-yr DJF in the North Atlantic between the two experiments (not shown). However, the higher density of FEAA trajectories in SMTHG than in CNTL over the 4th quadrant results in the reduction of the difference in the average water vapor of FEAA trajectories between CNTL and SMTHG. These results reveal that the difference in the spatial distribution of FEAA trajectories, not the difference in the distribution of water vapor in the North Atlantic by the Gulf Stream, is important for the difference in the water vapor of FEAA trajectories between CNTL and SMTHG.

4. Discussion and conclusions

4a Discussion

In this section, we discuss the EAA trajectories over the North Pacific. Because there is also a western boundary current which is the Kuroshio, it is helpful in analyzing the response of EAA trajectories to the western boundary currents. To investigate the response of EAA trajectories to the Kuroshio, the following two experiments of AFES (Kuwano-Yoshida and Minobe 2017) are used: one with the observed daily SSTs (CNTL) and the other with smoothed SSTs over 120˚E–180˚, 25˚–55˚N (SMTHK). Figure 14 presents the averaged SST for 20-yr DJF for CNTL, SMTHK, and CNTL−SMTHK. The SSTs of CNTL are higher than SMTHK widely from the East China Sea to the eastern side of Japan (Fig. 14c). The tracking and selecting process of EAA trajectories over the North Pacific is the same as the case of the North Atlantic introduced in section 2. However, the starting points of air parcels are arranged over 120˚E–135˚W, 15˚–50˚N.

Figure 15 represents the spatial distribution of EAA trajectories when they are located at 900 hPa for the 20-yr winters. The EAA trajectories of the North Pacific are distributed more widely than that of the North Atlantic (Figs. 15a and 15b). The characteristic of EAA trajectories distributed eastward in a smoothed SST experiment than in the CNTL experiment is the same with the case of the North Atlantic. Also, similar to the North Atlantic, a larger number of EAA trajectories are located on the SST front of the western boundary current in CNTL than in SMTHK (Fig. 15c). However, as opposed to the North Atlantic, there is no statistically significant difference in the number of EAA trajectories over the Kuroshio between CNTL and SMTHK.

No statistical difference in the number of EAA trajectories over the Kuroshio means that the effects of the Kuroshio on the EAA trajectories are weaker than that of the Gulf Stream. Many previous studies suggest that the SST gradient by the western boundary currents is important in the intensification of midlatitude atmosphere phenomena and ETCs (Nakamura et al. 2008; Sampe et al. 2010; Ma et al. 2016; Zhang et al. 2020). However, Tsopouridis et al. (2020) argued that the increase of LHF, SHF, and cyclone density by the Gulf Stream is greater than the increase by the Kuroshio. From these previous studies, the reason for the less effect of the western boundary current on the EAA trajectories in the North Pacific than in the North Atlantic is speculated as the weaker SST gradient by the Kuroshio than that of the Gulf Stream reported by previous studies (Nakamura et al. 2004; Tsopouridis et al. 2020). In order to get a meaningful difference in the North Pacific, a longer integration period than 20 years or an experiment with different settings will be needed.

4b Conclusions

To understand the response of EAA trajectories to the Gulf Stream, the air parcels on the North Atlantic from the DJF of 1981 to 2001 are tracked for 72 hours using the output of two experiments of AFES: one with observed SST data (CNTL) and the other with smoothed SST over the Gulf Stream SST front. The trajectories reaching above 900 hPa in the 48 hours of the largest ascent, and entering the area of an ETC are identified as EAA trajectories.

The EAA trajectories are mainly distributed near the Gulf Stream when EAA trajectories are located at 900 hPa in CNTL (Fig. 4b and 4c). This result agrees with the spatial distribution of the starting point of the rapidly ascending airstream of ETCs in previous studies (Eckhardt et al. 2004; Madonna et al. 2014). The difference in the number of EAA trajectories between CNTL and SMTHG is concentrated in the Gulf Stream current axis and the number of EAA trajectories is slightly larger in CNTL than in SMTHG over the Gulf Stream current axis (Fig. 4c). To investigate how the Gulf Stream affects the movement of air parcels in ETCs, the horizontal and vertical movement of the frontal EAA trajectories is investigated. The number of frontal EAA trajectories reaching above 300 (400) hPa is 31 (15) % larger in CNTL than in SMTHG, and the number of the frontal EAA trajectories reaching the stratosphere is 22 % higher in CNTL than in SMTHG (Fig. 8a and Table 1). Also, the number of frontal EAA trajectories that have moved more than 3000 km horizontally is 24 % larger in CNTL than in SMTHG (Fig. 9a). Because the correlation coefficient between movement distance and the reached height is 0.5 in both experiments, the reason for the longer movement distance of FEAA trajectories in CNTL is probably the faster wind speed at higher altitudes.

In the difference in the ascent of FEAA trajectories between the two experiments, diabatic heating plays an important role. The contribution of diabatic ascent to the difference in the ascent of FEAA trajectories between CNTL and SMTHG is 68 % (Table 2). Several previous studies have reported the importance of diabatic heating in the ascent of airstreams in ETCs (Madonna et al. 2014; Oertel et al. 2019; Saffin et al. 2021). The diabatic heating of FEAA trajectories in CNTL is 18 % stronger than that of SMTHG. Before crossing 900 hPa, the heating by vertical diffusion is dominant, but latent heating is important in the difference in the diabatic heating after crossing 900 hPa (Fig. 10c). The difference in the heating of FEAA trajectories in CNTL than in SMTHG is related to sensible and latent heat flux. The stronger sensible and latent heat flux over the Gulf Stream region intensifies heating by vertical diffusion and moisture supply in FEAA trajectories (Fig. 11). In order to investigate where the additional moisture of FEAA trajectories in CNTL than in SMTHG is mainly supplied, we calculated the contribution of 4 areas centered on 55°W and 43°N to the difference in the q of FEAA trajectories between CNTL and SMTHG (Fig. 13b and 13d). The 3rd quadrant where the Gulf Stream is located and where the FEAA trajectories are most distributed had the highest contribution. This result suggests that the difference in the spatial distribution of FEAA trajectories by the Gulf Stream between the two experiments is important in the moisture supply.

There are several studies about the interaction between the Gulf Stream and upward wind above Gulf Stream in winter (Minobe et al. 2008; Minobe et al. 2010; Kuwano-Yoshida et al. 2010). They showed that there is strong upward wind over the Gulf Stream rainband on the lower troposphere. Kuwano-Yoshida et al. (2010) suggested that the strong upward wind below 700 hPa in the Gulf Stream results from the cumulus convection through AGCM experiments. However, they couldn't find the effect of the Gulf Stream on the upward wind in the upper troposphere. Although the present study is limited to airstreams in ETCs, revealed that the Gulf Stream intensifies the upward motion of the ascending airstreams by using the air parcel tracking method. Because previous studies focus on the time-mean field of upward wind, they couldn't find that the Gulf Stream affects the characteristics of airstreams in ETCs under the MABL and facilitates the upward motion even to the upper troposphere. This study shed new light on midlatitude air-sea interaction by suggesting the mechanism by which the Gulf Stream influences the upward wind of the middle and upper troposphere.

Acknowledgement

I would like to express my gratitude to my supervisor, Prof. Shosiro Minobe. Without his support, I couldn’t start the research on air-sea interaction. Also, I wish to express my appreciation to my Ph.D. committee, Profs. Yoshinori Sasaki, Masaru Inatsu, Yousuke Sato, and Yoshida Akira. The comments and suggestions from the Ph.D. committee were very useful to improve my research. I’m grateful to my friends who have shared both sorrow and joy, especially members of G-day. Finally, I want to record my gratitude to my parents, Sookil Son and Sunlye Ha.

References

Binder, Hanin, Maxi Boettcher, Hanna Joos, and Heini Wernli. 2016. “The Role of Warm Conveyor Belts for the Intensification of Extratropical Cyclones in Northern Hemisphere Winter.” *Journal of the Atmospheric Sciences* 73 (10): 3997–4020.

Booth, James F., Luanne Thompson, Jérôme Patoux, and Kathryn A. Kelly. 2012. “Sensitivity of Midlatitude Storm Intensification to Perturbations in the Sea Surface Temperature near the Gulf Stream.” *Monthly Weather Review* 140 (4): 1241–56.

Boutle, I. A., R. J. Beare, S. E. Belcher, A. R. Brown, and R. S. Plant. 2010. “The Moist Boundary Layer under a Mid-Latitude Weather System.” *Boundary - Layer Meteorology* 134 (3): 367–86.

Brayshaw, David James, Brian Hoskins, and Michael Blackburn. 2011. “The Basic Ingredients of the North Atlantic Storm Track. Part II: Sea Surface Temperatures.” *Journal of the Atmospheric Sciences*. https://doi.org/10.1175/2011jas3674.1.

Browning, Keith A. 1986. “Conceptual Models of Precipitation Systems.” *Weather and Forecasting* 1 (1): 23–41.

Dacre, H. F., O. Martínez-Alvarado, and C. O. Mbengue. 2019. “Linking Atmospheric Rivers and Warm Conveyor Belt Airflows.” *Journal of Hydrometeorology*. https://doi.org/10.1175/jhm-d-18-0175.1.

Eckhardt, Sabine, Andreas Stohl, Heini Wernli, Paul James, Caroline Forster, and Nicole Spichtinger. 2004. “A 15-Year Climatology of Warm Conveyor Belts.” *Journal of Climate*. https://doi.org/10.1175/1520-0442(2004)017<0218:aycowc>2.0.co;2.

Emanuel, Kerry A., and Marina Živković-Rothman. 1999. “Development and Evaluation of a Convection Scheme for Use in Climate Models.” *Journal of the Atmospheric Sciences*. https://doi.org/10.1175/1520-0469(1999)056<1766:daeoac>2.0.co;2.

Enomoto, Takeshi, Akira Kuwano-Yoshida, Nobumasa Komori, and Wataru Ohfuchi. 2008. “Description of AFES 2: Improvements for High-Resolution and Coupled Simulations.” *High Resolution Numerical Modelling of the Atmosphere and Ocean*. https://doi.org/10.1007/978-0-387-49791-4_5.

Grams, Christian M., Linus Magnusson, and Erica Madonna. 2018. “An Atmospheric Dynamics Perspective on the Amplification and Propagation of Forecast Error in Numerical Weather Prediction Models: A Case Study.” *Quarterly Journal of the Royal Meteorological Society* 144 (717): 2577–91.

Hauser, Seraphine, Christian M. Grams, Michael J. Reeder, Shayne McGregor, Andreas H. Fink, and Julian F. Quinting. 2020. “A Weather System Perspective on Winter–spring Rainfall Variability in Southeastern Australia during El Niño.” *Quarterly Journal of the Royal Meteorological Society* 146 (731): 2614–33.

Hawcroft, M. K., L. C. Shaffrey, K. I. Hodges, and H. F. Dacre. 2012. “How Much Northern Hemisphere Precipitation Is Associated with Extratropical Cyclones?” *Geophysical Research Letters* 39 (24). https://doi.org/10.1029/2012gl053866.

Hersbach, Hans, Bill Bell, Paul Berrisford, Shoji Hirahara, András Horányi, Joaquín Muñoz-Sabater, Julien Nicolas, et al. 2020. “The ERA5 Global Reanalysis.” *Quarterly Journal of the Royal Meteorological Society* 146 (730): 1999–2049.

Hirata, Hidetaka, Ryuichi Kawamura, Masaya Kato, and Taro Shinoda. 2015. “Influential Role of Moisture Supply from the Kuroshio/Kuroshio Extension in the Rapid Development of an Extratropical Cyclone.” *Monthly Weather Review* 143 (10): 4126–44.

Joos, H., and R. M. Forbes. 2016. "Impact of Different IFS Microphysics on a Warm Conveyor Belt and the Downstream Flow Evolution." *Quarterly Journal of the Royal Meteorological Society*. https://doi.org/10.1002/qj.2863.

Joos, H., and H. Wernli. 2012. "Influence of Microphysical Processes on the Potential Vorticity Development in a Warm Conveyor Belt: A Case-Study with the Limited-Area Model COSMO." *Quarterly Journal of the Royal Meteorological Society* 138 (663): 407–18.

Joyce, Terrence M., Young-oh Kwon, Hyodae Seo, and Caroline C. Ummenhofer. 2019. "Meridional Gulf Stream Shifts Can Influence Wintertime Variability in the North Atlantic Storm Track and Greenland Blocking." *Geophysical Research Letters* 46 (3): 1702–8.

Kunkel, Kenneth E., David R. Easterling, David A. R. Kristovich, Byron Gleason, Leslie Stoecker, and Rebecca Smith. 2010. "Recent Increases in U.S. Heavy Precipitation Associated with Tropical Cyclones." *Geophysical Research Letters* 37 (24). https://doi.org/10.1029/2010gl045164.

Kuwano-Yoshida, Akira, Takeshi Enomoto, and Wataru Ohfuchi. 2010. "An Improved PDF Cloud Scheme for Climate Simulations." *Quarterly Journal of the Royal Meteorological Society*. https://doi.org/10.1002/qj.660.

Kuwano-Yoshida, Akira, and Shoshiro Minobe. 2017. "Storm-Track Response to SST Fronts in the Northwestern Pacific Region in an AGCM." *Journal of Climate* 30 (3): 1081–1102.

Kuwano-Yoshida, Akira, Shoshiro Minobe, and Shang-Ping Xie. 2010. "Precipitation Response to the Gulf Stream in an Atmospheric GCM." *Journal of Climate* 23 (13): 3676–98.

Kwon, Young-Oh, Michael A. Alexander, Nicholas A. Bond, Claude Frankignoul, Hisashi Nakamura, Bo Qiu, and Lu Anne Thompson. 2010. "Role of the Gulf Stream and Kuroshio–Oyashio Systems in Large-Scale Atmosphere–ocean Interaction: A Review." *Journal of Climate* 23 (12): 3249–81.

Larson, Joshua, Yaping Zhou, and R. Wayne Higgins. 2005. “Characteristics of Landfalling Tropical Cyclones in the United States and Mexico: Climatology and Interannual Variability.” *Journal of Climate* 18 (8): 1247–62.

Li, Xiaofan, C-H Sui, K-M Lau, and M-D Chou. 1999. “Large-Scale Forcing and Cloud–Radiation Interaction in the Tropical Deep Convective Regime.” *Journal of the Atmospheric Sciences*.

Madonna, Erica, Heini Wernli, Hanna Joos, and Olivia Martius. 2014. “Warm Conveyor Belts in the ERA-Interim Dataset (1979–2010). Part I: Climatology and Potential Vorticity Evolution.” *Journal of Climate*. https://doi.org/10.1175/jcli-d-12-00720.1.

Martínez-Alvarado, O., H. Joos, J. Chagnon, M. Boettcher, S. L. Gray, R. S. Plant, J. Methven, and H. Wernli. 2014. “The Dichotomous Structure of the Warm Conveyor Belt.” *Quarterly Journal of the Royal Meteorological Society*. https://doi.org/10.1002/qj.2276.

Masunaga, Ryusuke, Hisashi Nakamura, Bunmei Taguchi, and Takafumi Miyasaka. 2020. “Processes Shaping the Frontal-Scale Time-Mean Surface Wind Convergence Patterns around the Kuroshio Extension in Winter.” *Journal of Climate* 33 (1): 3–25.

Ma, Xiaohui, Ping Chang, R. Saravanan, Raffaele Montuoro, Hisashi Nakamura, Dexing Wu, Xiaopei Lin, and Lixin Wu. 2017. “Importance of Resolving Kuroshio Front and Eddy Influence in Simulating the North Pacific Storm Track.” *Journal of Climate* 30 (5): 1861–80.

Ma, Xiaohui, Zhao Jing, Ping Chang, Xue Liu, Raffaele Montuoro, R. Justin Small, Frank O. Bryan, et al. 2016. “Western Boundary Currents Regulated by Interaction between Ocean Eddies and the Atmosphere.” *Nature* 535 (7613): 533–37.

Minobe, Shoshiro, Akira Kuwano-Yoshida, Nobumasa Komori, Shang-Ping Xie, and Richard Justin Small. 2008. “Influence of the Gulf Stream on the Troposphere.” *Nature* 452 (7184): 206–9.

Minobe, Shoshiro, Masato Miyashita, Akira Kuwano-Yoshida, Hiroki Tokinaga, and Shang-Ping Xie. 2010. “Atmospheric Response to the Gulf Stream: Seasonal Variations.” *Journal of Climate* 23 (13): 3699–3719.

Nakamura, Hirohiko, Ayako Nishina, and Shoshiro Minobe. 2012. “Response of Storm Tracks to Bimodal Kuroshio Path States South of Japan.” *Journal of Climate* 25 (21): 7772–79.

Nakamura, Hisashi, Takeaki Sampe, Atsushi Goto, Wataru Ohfuchi, and Shang-Ping Xie. 2008. “On the Importance of Midlatitude Oceanic Frontal Zones for the Mean State and Dominant Variability in the Tropospheric Circulation.” *Geophysical Research Letters*. https://doi.org/10.1029/2008gl034010.

Oertel, Annika, Maxi Boettcher, Hanna Joos, Michael Sprenger, and Heini Wernli. 2019. “Potential Vorticity Structure of Embedded Convection in a Warm Conveyor Belt and Its Relevance for the Large-Scale Dynamics.” *Weather and Climate Dynamics Discussions*, September, 1–38.

Ogawa, Fumiaki, Hisashi Nakamura, Kazuaki Nishii, Takafumi Miyasaka, and Akira Kuwano-Yoshida. 2012. “Dependence of the Climatological Axial Latitudes of the Tropospheric Westerlies and Storm Tracks on the Latitude of an Extratropical Oceanic Front: STORMTRACK/JET SENSITIVITY TO SST FRONT.” *Geophysical Research Letters* 39 (5). https://doi.org/10.1029/2011gl049922.

Ogawa, Fumiaki, and Thomas Spengler. 2019. “Prevailing Surface Wind Direction during Air–sea Heat Exchange.” *Journal of Climate* 32 (17): 5601–17.

Ohfuchi, W., and Coauthors, 2004: 10-km mesh meso-scale resolving simulations of the global atmosphere on the Earth Simulator—preliminary outcomes of AFES (AGCM for the Earth Simulator). J. Earth Simul., 1, 8–34.

Omrani, Nour-Eddine, Fumiaki Ogawa, Hisashi Nakamura, Noel Keenlyside, Sandro W. Lubis, and Katja Matthes. 2019. "Key Role of the Ocean Western Boundary Currents in Shaping the Northern Hemisphere Climate." *Scientific Reports* 9 (1): 3014.

Onogi, Kazutoshi, Junichi Tsutsui, Hiroshi Koide, Masami Sakamoto, Shinya Kobayashi, Hiroaki Hatsushika, Takanori Matsumoto, et al. 2007. "The JRA-25 Reanalysis." *Journal of the Meteorological Society of Japan* 85 (3): 369–432.

O'Reilly, Christopher H., and Arnaud Czaja. 2015. "The Response of the Pacific Storm Track and Atmospheric Circulation to Kuroshio Extension Variability: Response of Storm Tracks to Kuroshio Extension Variability." *Quarterly Journal of the Royal Meteorological Society* 141 (686): 52–66.

O'Reilly, Christopher H., Shoshiro Minobe, and Akira Kuwano-Yoshida. 2016. "The Influence of the Gulf Stream on Wintertime European Blocking." *Climate Dynamics* 47 (5-6): 1545–67.

O'Reilly, Christopher H., Shoshiro Minobe, Akira Kuwano-Yoshida, and Tim Woollings. 2017. "The Gulf Stream Influence on Wintertime North Atlantic Jet Variability." *Quarterly Journal of the Royal Meteorological Society* 143 (702): 173–83.

Pfahl, Stephan, Erica Madonna, Maxi Boettcher, Hanna Joos, and Heini Wernli. 2014. "Warm Conveyor Belts in the ERA-Interim Dataset (1979–2010). Part II: Moisture Origin and Relevance for Precipitation." *Journal of Climate* 27 (1): 27–40.

Piazza, Marie, Laurent Terray, Julien Boé, Eric Maisonnave, and Emilia Sanchez-Gomez. 2016. "Influence of Small-Scale North Atlantic Sea Surface Temperature Patterns on the Marine Boundary Layer and Free Troposphere: A Study Using the Atmospheric ARPEGE Model." *Climate Dynamics* 46 (5-6): 1699–1717.

Priestley, Matthew D. K., and Jennifer L. Catto. 2022. "Future Changes in the Extratropical Storm Tracks and Cyclone Intensity, Wind Speed, and Structure." *Weather and Climate Dynamics* 3 (1): 337–60.

Reynolds, Richard W., Thomas M. Smith, Chunying Liu, Dudley B. Chelton, Kenneth S. Casey, and Michael G. Schlax. 2007. "Daily High-Resolution-Blended Analyses for Sea Surface Temperature." *Journal of Climate* 20 (22): 5473–96.

Rio, M-H, S. Mulet, and N. Picot. 2014. "Beyond GOCE for the Ocean Circulation Estimate: Synergetic Use of Altimetry, Gravimetry, and in Situ Data Provides New Insight into Geostrophic and Ekman Currents." *Geophysical Research Letters*. https://doi.org/10.1002/2014gl061773.

Rodwell, M. J., M. Drévillon, C. Frankignoul, J. W. Hurrell, H. Pohlmann, M. Stendel, and R. T. Sutton. 2004. "North Atlantic Forcing of Climate and Its Uncertainty from a Multi-Model Experiment." *Quarterly Journal of the Royal Meteorological Society*. https://doi.org/10.1256/qj.03.207.

Saffin, Leo, John Methven, Jake Bland, Ben Harvey, and Claudio Sanchez. 2021. "Circulation Conservation in the Outflow of Warm Conveyor Belts and Consequences for Rossby Wave Evolution." *Quarterly Journal of the Royal Meteorological Society* 147 (740): 3587–3610.

Sampe, Takeaki, Hisashi Nakamura, Atsushi Goto, and Wataru Ohfuchi. 2010. "Significance of a Midlatitude SST Frontal Zone in the Formation of a Storm Track and an Eddy-Driven Westerly Jet*." *Journal of Climate*. https://doi.org/10.1175/2009jcli3163.1.

Schäfler, Andreas, and Florian Harnisch. 2015. "Impact of the Inflow Moisture on the Evolution of a Warm Conveyor Belt." *Quarterly Journal of the Royal Meteorological Society* 141 (686): 299–310.

Schultz, David M., and Geraint Vaughan. 2011. "Occluded Fronts and the Occlusion Process: A Fresh Look at Conventional Wisdom." *Bulletin of the American Meteorological Society* 92 (4): 443–66.

Scoccimarro, Enrico, Silvio Gualdi, Gabriele Villarini, Gabriel A. Vecchi, Ming Zhao, Kevin Walsh, and Antonio Navarra. 2014. "Intense Precipitation Events Associated with Landfalling Tropical Cyclones in Response to a Warmer Climate and Increased CO2." *Journal of Climate* 27 (12): 4642–54.

Sheldon, Luke, Arnaud Czaja, Benoit Vannière, Cyril Morcrette, Benoit Sohet, Mathieu Casado, and Doug Smith. 2017. "A 'warm Path' for Gulf Stream–troposphere Interactions." *Tellus A: Dynamic Meteorology and Oceanography*. https://doi.org/10.1080/16000870.2017.1299397.

Shimada, Teruhisa, and Shoshiro Minobe. 2011. "Global Analysis of the Pressure Adjustment Mechanism over Sea Surface Temperature Fronts Using AIRS/Aqua Data." *Geophysical Research Letters* 38 (6). https://doi.org/10.1029/2010gl046625.

Sinclair, V. A., S. L. Gray, and S. E. Belcher. 2008. "Boundary-Layer Ventilation by Baroclinic Life Cycles." *Quarterly Journal of the Royal Meteorological Society* 134 (635): 1409–24.

Small, R. J., S. P. deSzoeke, S. P. Xie, L. O'Neill, H. Seo, Q. Song, P. Cornillon, M. Spall, and S. Minobe. 2008. "Air–sea Interaction over Ocean Fronts and Eddies." *Dynamics of Atmospheres and Oceans* 45 (3-4): 274–319.

Small, R. Justin, Frank O. Bryan, Stuart P. Bishop, and Robert A. Tomas. 2019. "Air–sea Turbulent Heat Fluxes in Climate Models and Observational Analyses: What Drives Their Variability?" *Journal of Climate* 32 (8): 2397–2421.

Small, R. Justin, Robert A. Tomas, and Frank O. Bryan. 2014. "Storm Track Response to Ocean Fronts in a Global High-Resolution Climate Model." *Climate Dynamics* 43 (3-4): 805–28.

Sprenger, M., and H. Wernli. 2015. “The LAGRANTO Lagrangian Analysis Tool – Version 2.0.” *Geoscientific Model Development*. https://doi.org/10.5194/gmd-8-2569-2015.

Steinfeld, Daniel, Maxi Boettcher, Richard Forbes, and Stephan Pfahl. 2020. “The Sensitivity of Atmospheric Blocking to Upstream Latent Heating – Numerical Experiments.” *Weather and Climate Dynamics* 1 (2): 405–26.

Steinfeld, Daniel, and Stephan Pfahl. 2019. “The Role of Latent Heating in Atmospheric Blocking Dynamics: A Global Climatology.” *Climate Dynamics* 53 (9-10): 6159–80.

Stohl, Andreas. 2001. “A 1-Year Lagrangian ‘climatology’ of Airstreams in the Northern Hemisphere Troposphere and Lowermost Stratosphere.” *Journal of Geophysical Research* 106 (D7): 7263–79.

Tsopouridis, Leonidas, Thomas Spengler, and Clemens Spensberger. 2020. “SST Fronts along the Gulf Stream and Kuroshio Affect the Winter Climatology Primarily in the Absence of Cyclones.” *Weather and Climate Dynamics Discussions*, preprint, https://doi.org/10.5194/wcd-2020-50.

Vannière, Benoît, Malcolm Roberts, Pier Luigi Vidale, Kevin Hodges, Marie-Estelle Demory, Louis-Philippe Caron, Enrico Scoccimarro, Laurent Terray, and Retish Senan. 2020. “The Moisture Budget of Tropical Cyclones in HighResMIP Models: Large-Scale Environmental Balance and Sensitivity to Horizontal Resolution.” *Journal of Climate* 33 (19): 8457–74.

Vries, Hylke de, Sebastian Scher, Rein Haarsma, Sybren Drijfhout, and Aarnout van Delden. 2019. “How Gulf-Stream SST-Fronts Influence Atlantic Winter Storms.” *Climate Dynamics* 52 (9-10): 5899–5909.

Wernli, Heini, and Huw C. Davies. 1997. “A Lagrangian-based Analysis of Extratropical Cyclones. I: The Method and Some Applications.” *Quarterly Journal of the Royal Meteorological Society* 123 (538): 467–89.

Wernli, Heini, and Cornelia Schwierz. 2006. "Surface Cyclones in the ERA-40 Dataset (1958–2001). Part I: Novel Identification Method and Global Climatology." *Journal of the Atmospheric Sciences* 63 (10): 2486–2507.

Wilson, Chris, Bablu Sinha, and Richard G. Williams. 2009. "The Effect of Ocean Dynamics and Orography on Atmospheric Storm Tracks." *Journal of Climate* 22 (13): 3689–3702.

Yamamoto, Ayako, Masami Nonaka, Patrick Martineau, Akira Yamazaki, Young-Oh Kwon, Hisashi Nakamura, and Bunmei Taguchi. 2021. "Oceanic Moisture Sources Contributing to Wintertime Euro-Atlantic Blocking." *Weather and Climate Dynamics* 2 (3): 819–40.

Zhang, Chao, Hailong Liu, Jinbo Xie, Pengfei Lin, Chongyin Li, Qian Yang, and Jie Song. 2020. "North Pacific Storm Track Response to the Mesoscale SST in a Global High-Resolution Atmospheric Model." *Climate Dynamics*. https://doi.org/10.1007/s00382-020-05343-x.

Zhang, Xingzhi, Xiaohui Ma, and Lixin Wu. 2019. "Effect of Mesoscale Oceanic Eddies on Extratropical Cyclogenesis: A Tracking Approach." *Journal of Geophysical Research* 124 (12): 6411–22.

Tables

Table 1. The number of the FEAA trajectories having 48 hours or more recorded after the 900 hPa crossing in units of 1,000.

	All	Reaching 300 hPa	Reaching 400 hPa	Reaching 2 PVU
CNTL	4,073	643	2,097	353
SMTHG	3,838	489	1,817	290
(CNTL−SMTHG) /SMTHG	6 %	31 %	15 %	22 %

Table 2. Average of diabatic and adiabatic ascent of all FEAA trajectories in each experiment in units of hPa.

	diabatic	adiabatic	diabatic + adiabatic
CNTL	265.4	209.6	475.0
SMTHG	253.1	203.8	456.9
CNTL−SMTHG	12.3	5.8	18.1

Figures

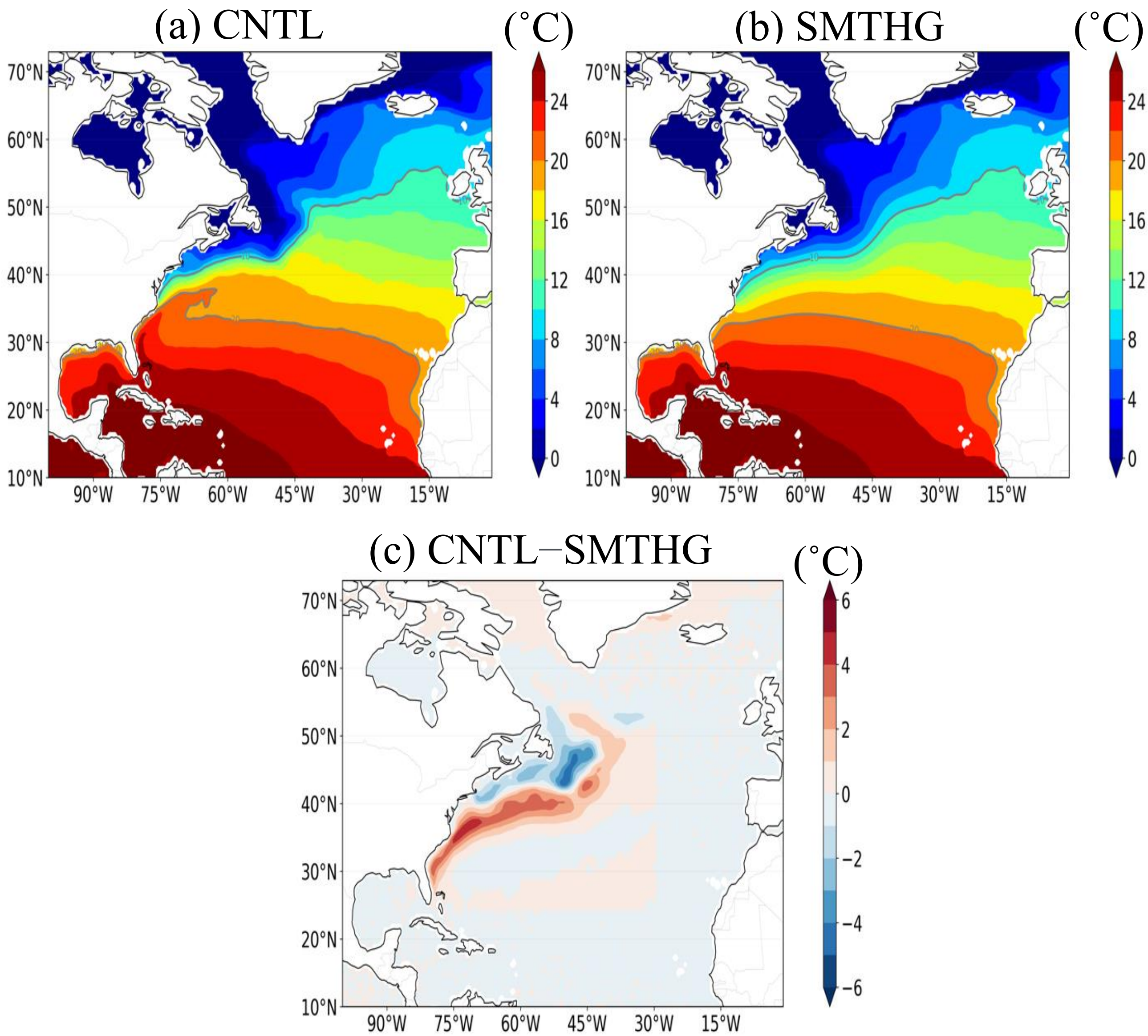

Fig. 1. Climatological SSTs in DJF for (a) CNTL (b) SMTHG and (c) their difference (˚C). The gray contours represent 10˚C and 20˚C in (a) and (b).

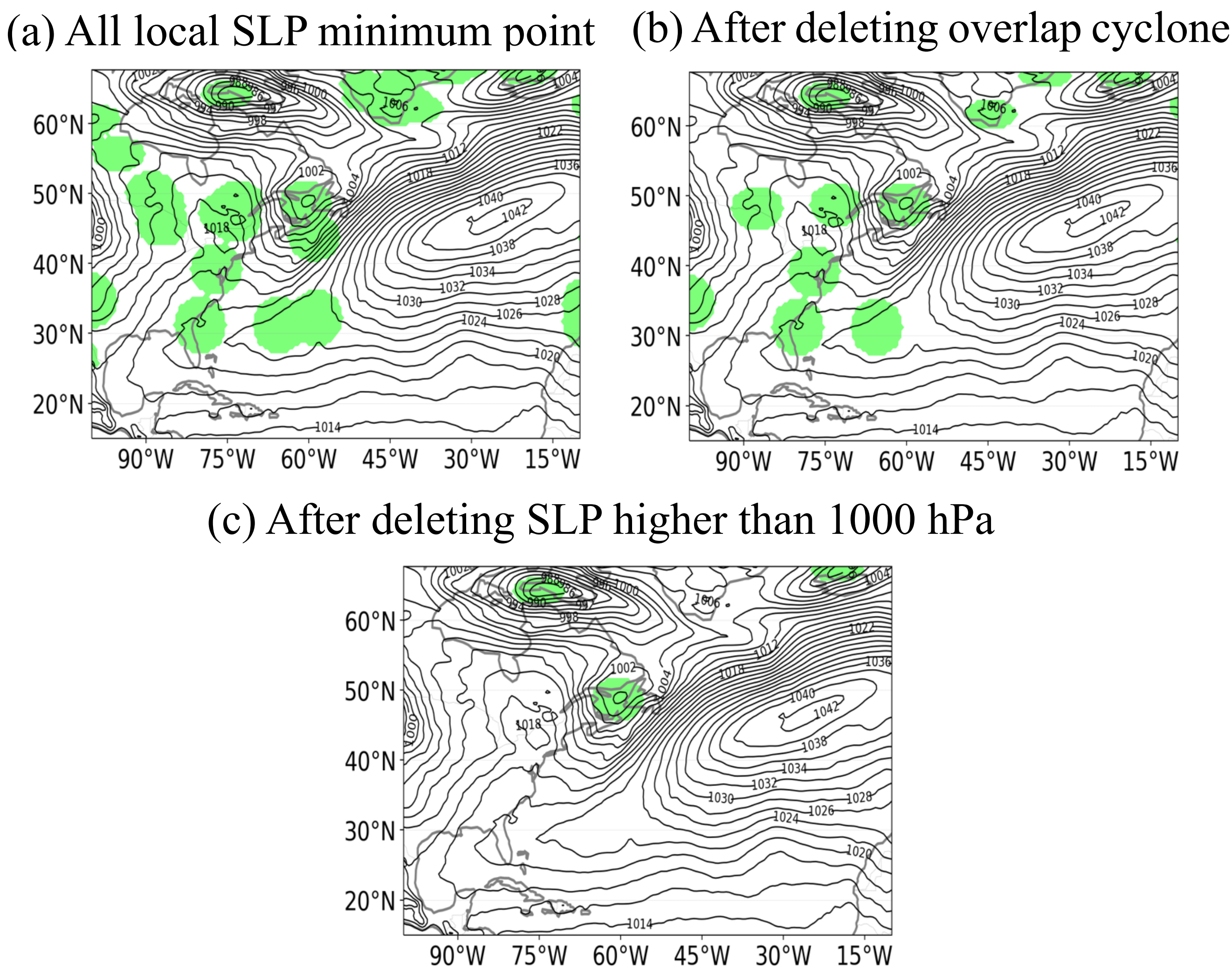

Fig. 2. Illustration of detection of cyclone areas of CNTL in 03:00 UTC 01 December 1981 for (a) all local SLP minimum points and cyclone areas, (b) cyclone areas after deleting overlap cyclones from (a), and (c) cyclone areas after deleting SLP higher than 1000 hPa from (b). The gray and black lines represent coastal lines and sea level pressure. The green circles indicate areas of cyclones.

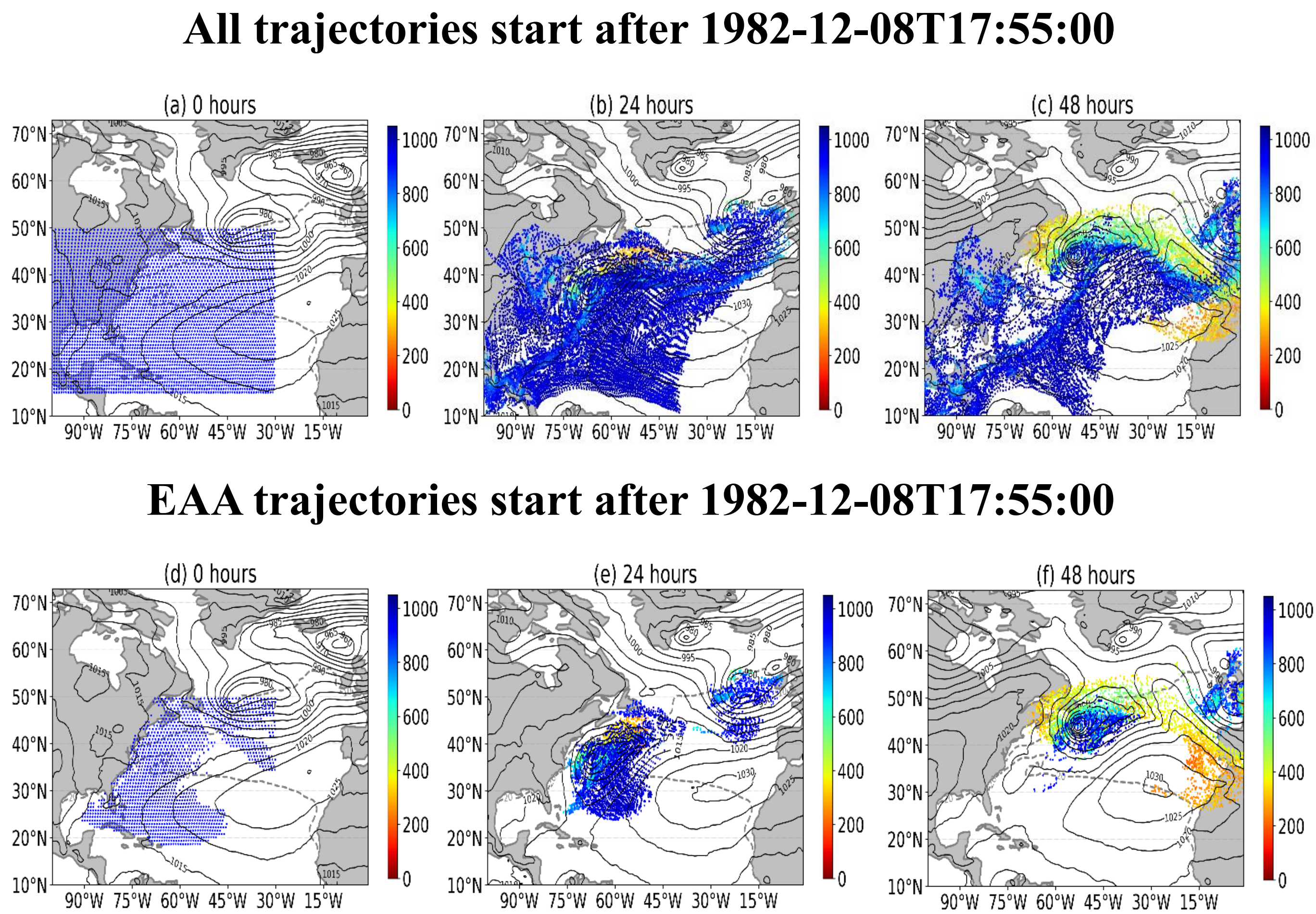

Fig. 3. Horizontal positions and heights (hPa) of all trajectories in (a) 0, (b) 24, and (c) 48 hours after starting at 1755 UTC 08 December 1982, and those for EAA trajectories (d) – (f). Dashed gray contours indicate SSTs of 10˚C and 20˚C The black contour represents sea level pressure in units of hPa.

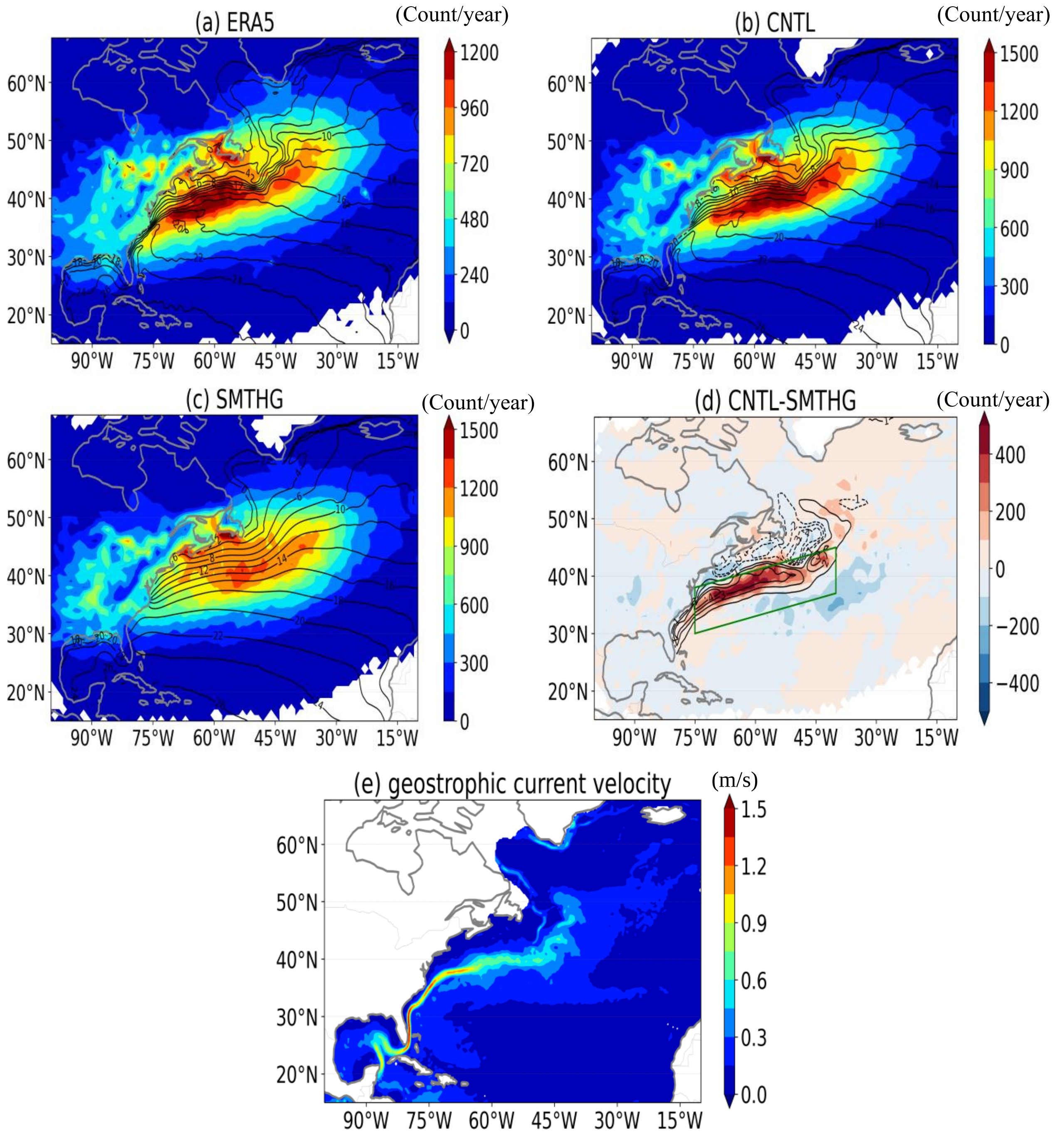

Fig. 4. Density (color shading) of EAA trajectories at 900 hPa given by the number of trajectories in 1x1-degree box per year for (a) ERA5 (b) CNTL, (c) SMTHG, and (d) the difference between CNTL and SMTHG. The black lines are contours of SSTs in units of °C. In (d) CNTL−SMTHG, the green box represents the Gulf Stream region. (e) Mean surface geostrophic current velocity averaged for 32 winter seasons by using the satellite altimetry data of Copernicus Marine Environment Monitoring Service (CMEMS; Rio et al. 2014).

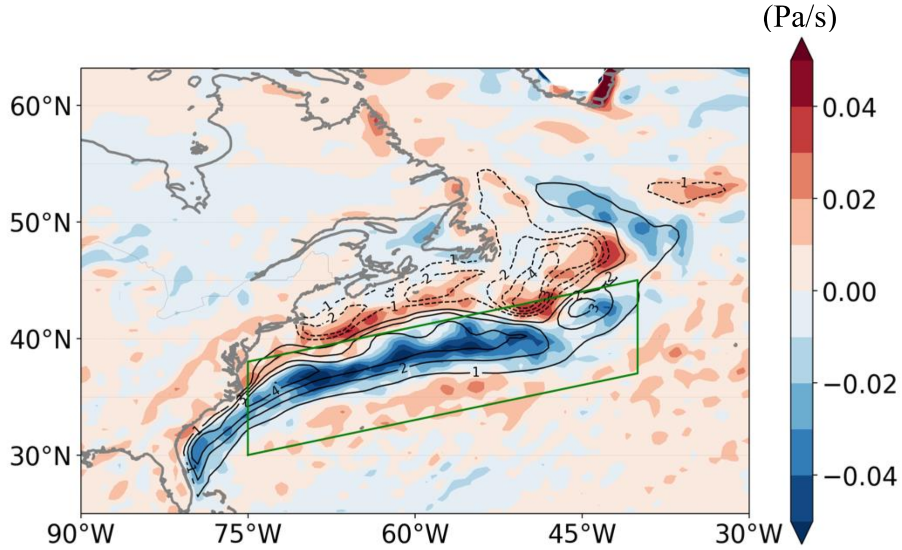

Fig. 5. The difference in the upward wind at 850 hPa in 20 winter seasons between CNTL and SMTHG. The gray and black line represents costal line and SST. The green box represents the Gulf Stream region.

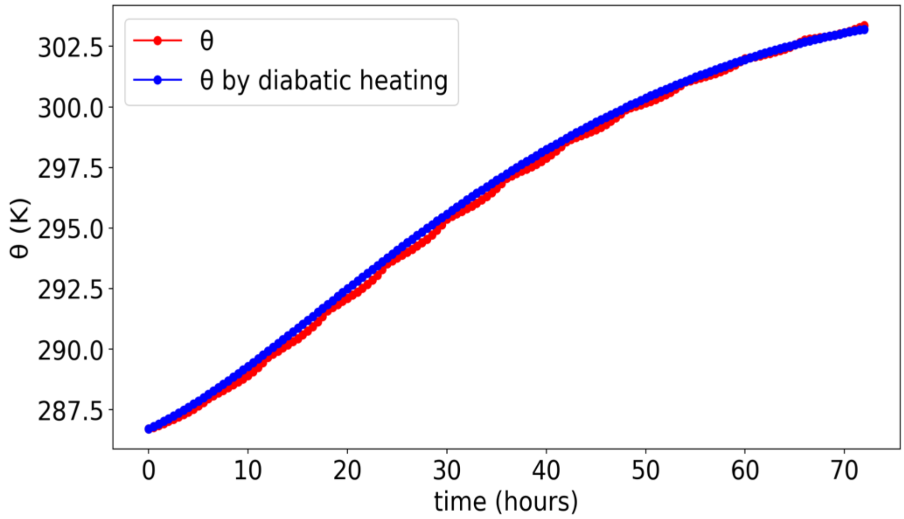

Fig. 6. Time evolution of potential temperature (θ) of average of FEAA trajectories after the tracking begins. The red lines represent the potential temperature tracked by the LAGRANTO, whereas the blue line represent the potential temperature estimated using diabatic heating.

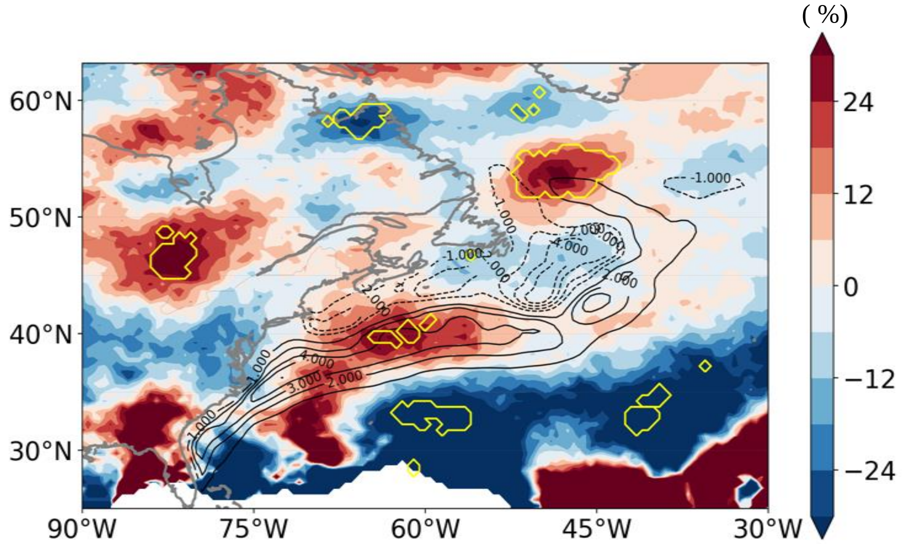

Fig. 7. The difference in the cyclone frequency in 20 winter seasons for CNTL−SMTHG. The gray and black line represents costal line and SST. The 95 % confidence level is shown by yellow contours.

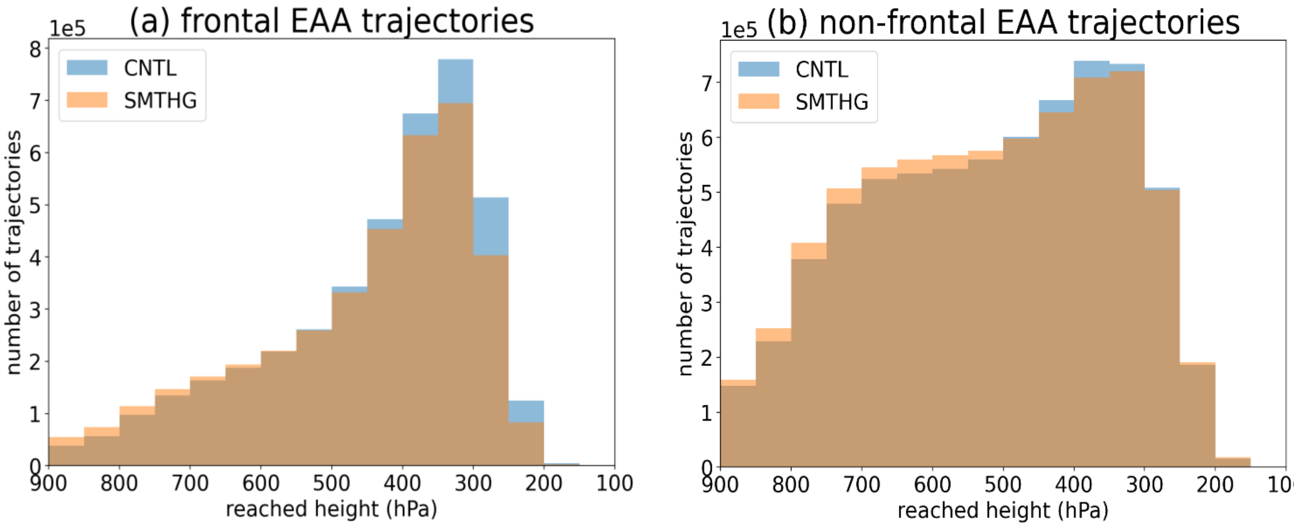

Fig. 8. The number of the EAA trajectories along with reached height for 48 hours after crossing 900 hPa for (a) frontal EAA trajectories and (b) non-frontal EAA trajectories. The x-axis is reached height of the frontal EAA trajectories for 48 hours and the y-axis is the number of EAA trajectories for 48 hours. The blue (orange) color shows a value of CNTL (SMTHG).

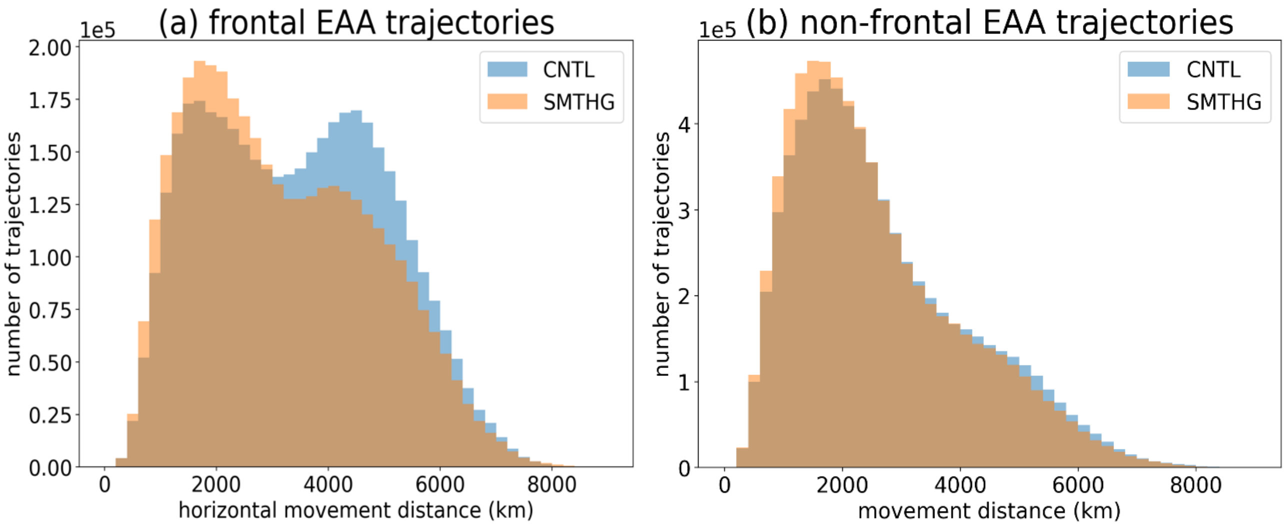

Fig. 9. The number of EAA trajectories along with movement distance for 48 hours after crossing 900 hPa for (a) frontal EAA trajectories and (b) non-frontal EAA trajectories. The x-axis represents movement distance for 48 hours. The y-axis represents a number of air parcel trajectories. The blue (orange) color shows a value of CNTL (SMTHG).

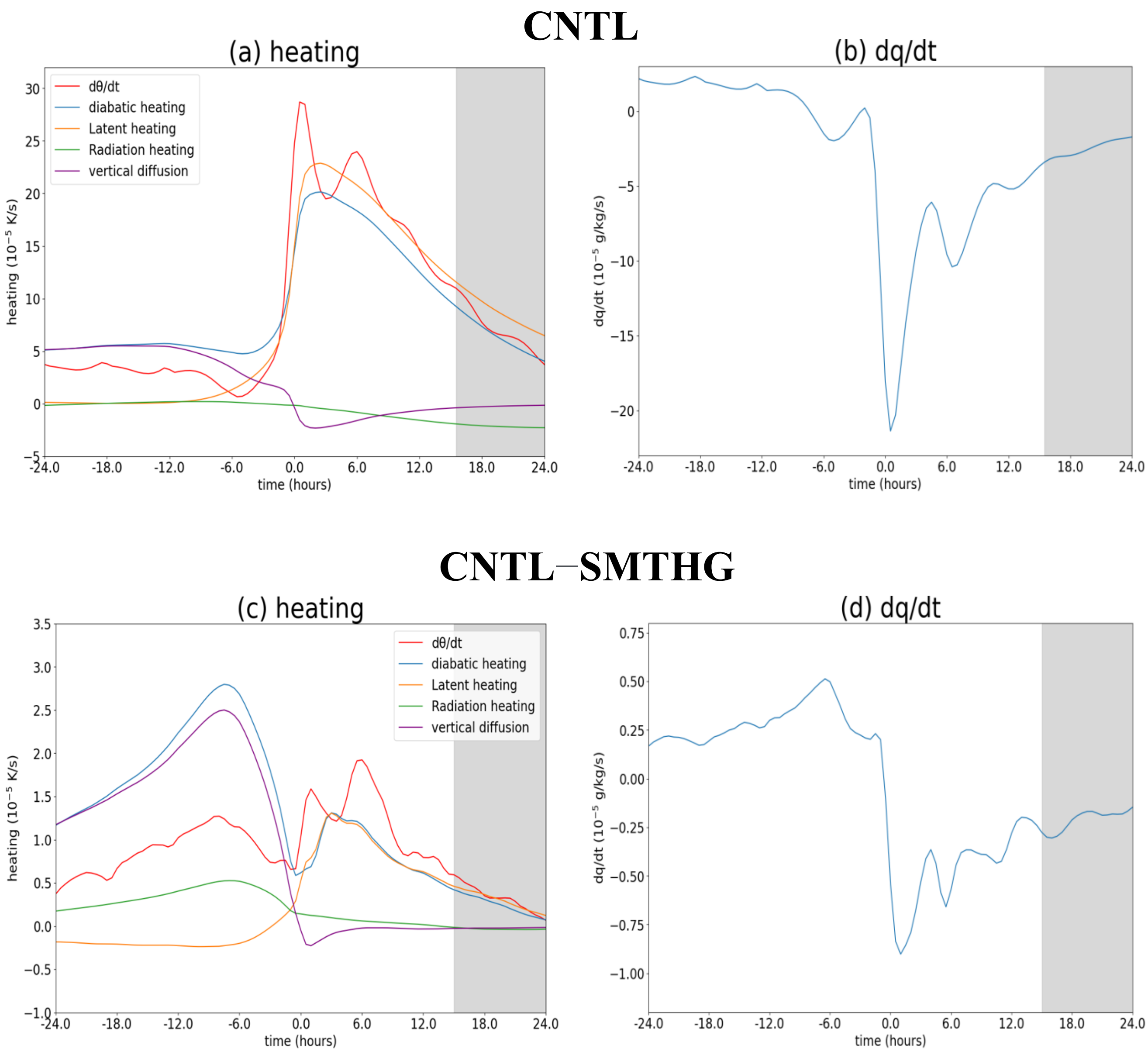

Fig. 10. Time evolution of (a) diabatic heating and (b) time derivative of specific humidity (q) in average of all FEAA trajectories. The 0 hours is the time when the trajectory first crosses 900 hPa. The red, cyan, orange, green, and brown lines represent the time derivative of θ, diabatic heating, latent heating, radiation heating, and vertical diffusion in units of 10^{-5} K/s. The gray areas represent the temporal range where less than 90 % of the trajectories exist. (c) and (d) is the same as (a) and (b), but for CNTL−SMTHG.

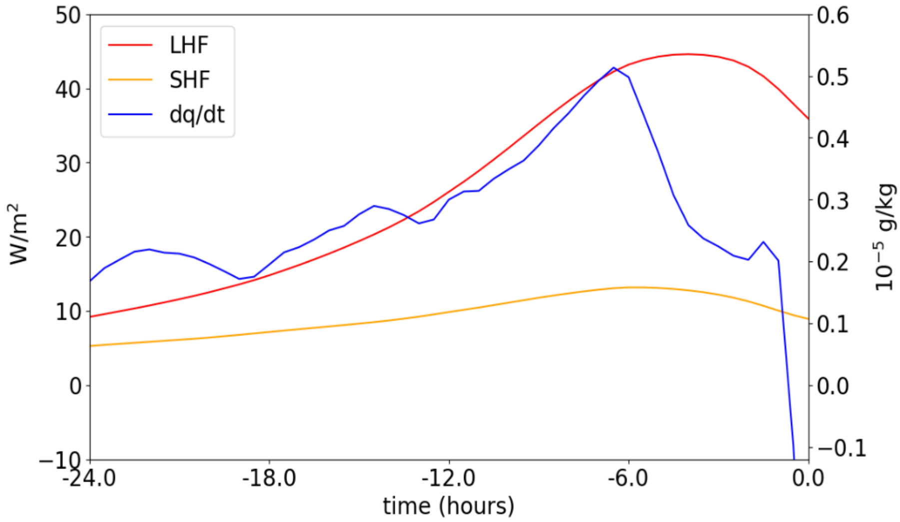

Fig. 11. Difference in the time evolution of latent (LHF) and sensible (SHF) heat fluxes, SHF, and the time derivative of specific humidity (dq/dt) of average of all FEAA trajectories between CNTL and SMTHG. The 0 hours of x-axis is the time when the FEAA trajectories first cross 900 hPa. The left y-axis is heat flux in units of W/m^2. The right y-axis is specific humidity in units of g/kg.

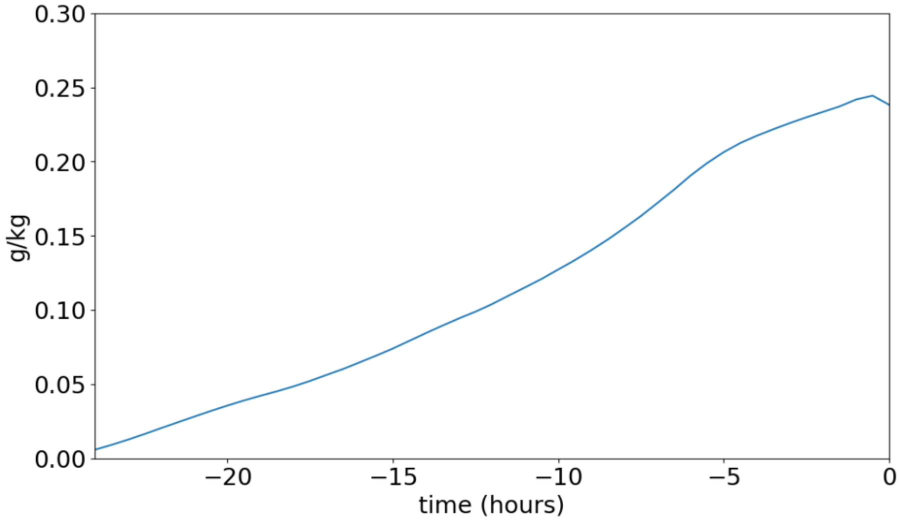

Fig. 12. Difference in the average specific humidity of all FEAA trajectories between CNTL and SMTHG. The 0 hours of x-axis is the time when the FEAA trajectories first cross 900 hPa. The y-axis is specific humidity in units of g/kg.

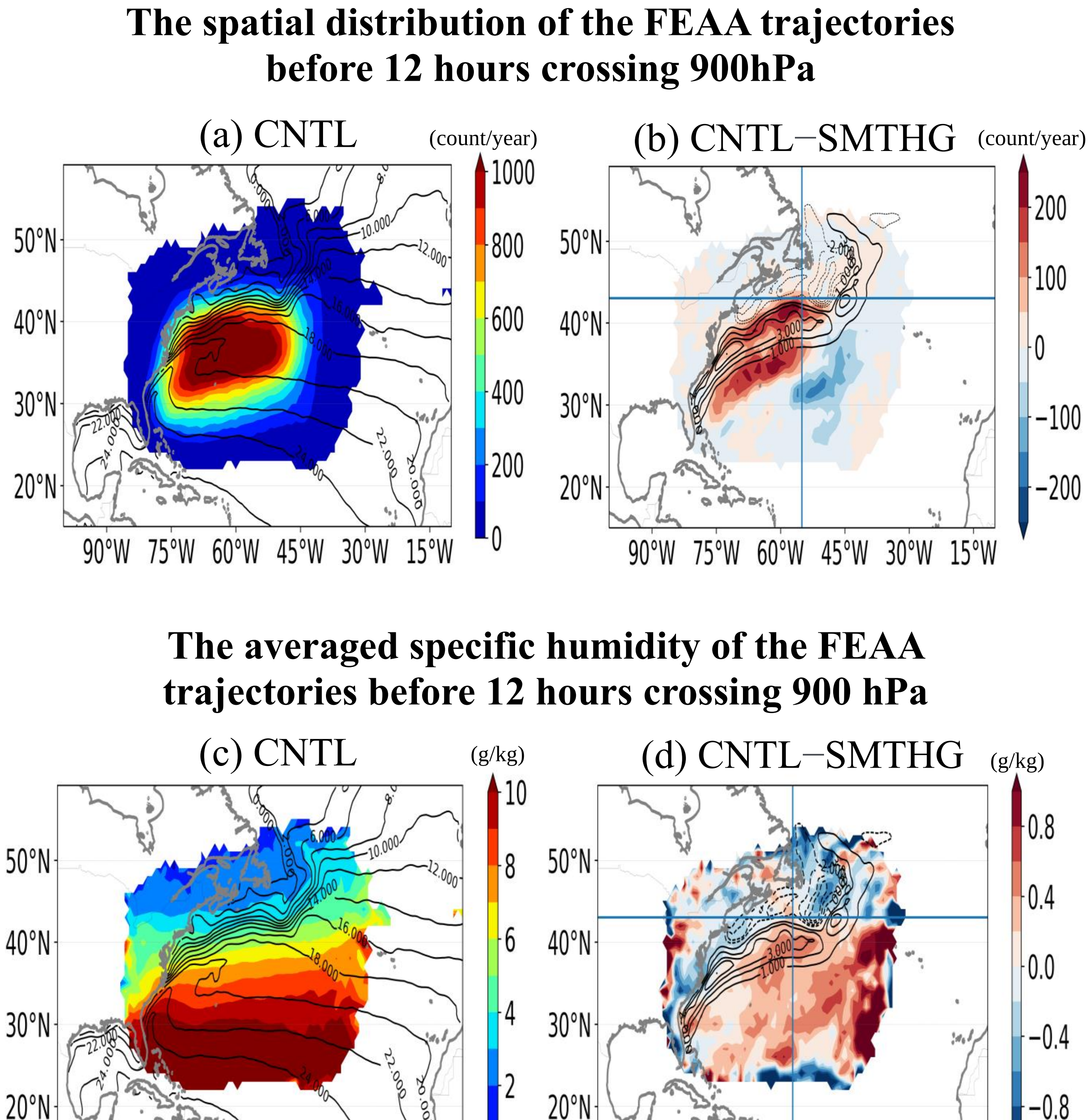

Fig 13. Spatial distribution of the FEAA trajectories before 12 hours crossing 900hPa first time for (a) CNTL and (b) CNTL−SMTHG. The gray line is coastal line. Black contours indicate SSTs in units of °C. The shading color represents the density of FEAA trajectories before 12 hours crossing 900hPa time firstly. The average specific humidity of the FEAA trajectories for (c) CNTL and (d) CNTL−SMTHG before 12 hours crossing 900hPa time firstly. The color shading is average specific humidity. The blue horizontal and vertical lines in (b) and (d) divide four quadrants used an analysis described in the main text.

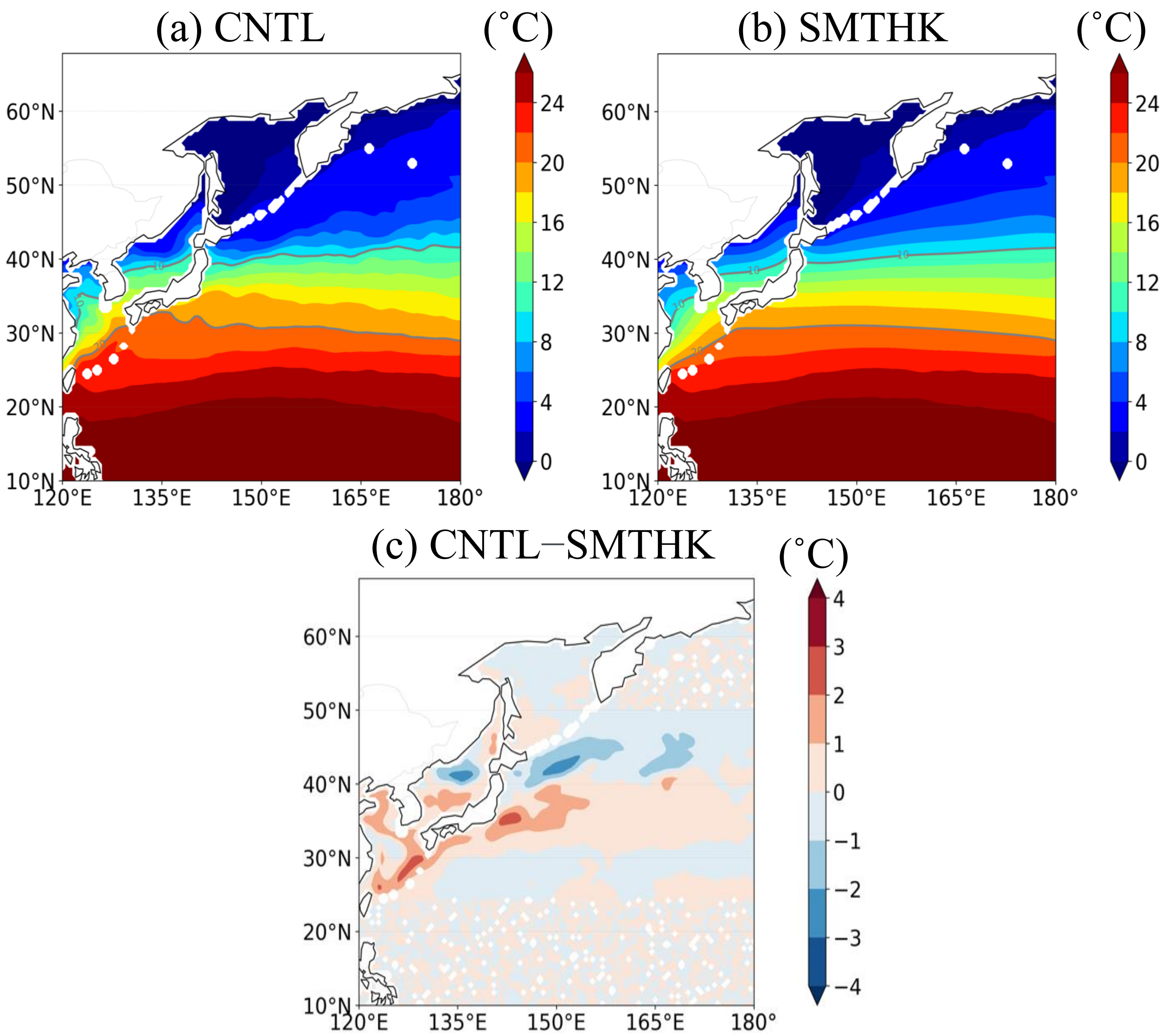

Fig. 14. Climatological SSTs in DJF over the North Pacific for (a) CNTL (b) SMTHK and (c) the difference between CNTL and SMTHK (˚C). The gray contours represent 10˚C and 20˚C.

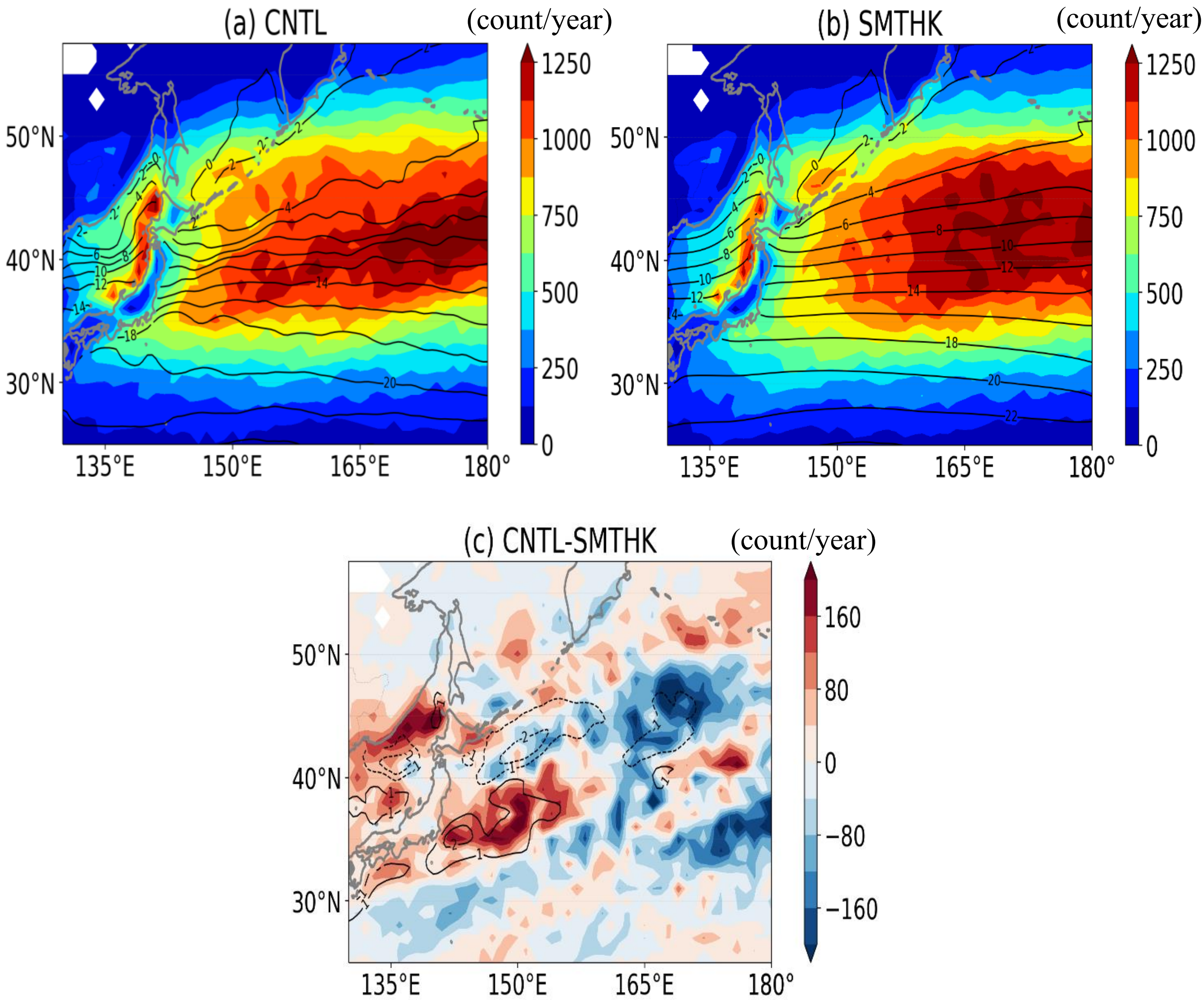

Fig. 15. Density (color shading) of EAA trajectories at 900 hPa given by the number of trajectories in 1x1-degree box per year for (a) CNTL, (b) SMTHK, and (c) the difference between CNTL and SMTHK. The black lines are contours of SSTs in units of °C.